Check for updates

METHOD ARTICLE

REVISED Development of an *in vitro* microfluidic model to study the role of microenvironmental cells in oral cancer metastasis [version 2; peer review: 2 approved]

Alice Scemama[1], Sophia Lunetto[2], Artysha Tailor[1], Stefania Di Cio[3], Matthew Dibble[3], Julien Gautrot[3], Adrian Biddle [ID][1]

[1]Blizard Institute, Queen Mary University of London, London, E1 2AT, UK
[2]Queen Mary University of London, London, England, UK
[3]School of Engineering and Materials Science, Queen Mary University of London, London, E1 4NS, UK

Abstract

Metastasis occurs when cancer cells leave the primary tumour and travel to a secondary site to form a new lesion. The tumour microenvironment (TME) is recognised to greatly influence this process, with for instance the vascular system enabling the dissemination of the cells into other tissues. However, understanding the exact role of these microenvironmental cells during metastasis has proven challenging. Indeed, *in vitro* models often appear too simplistic, and the study of the interactions between different cell types in a 3D space is limited. On the other hand, even though *in vivo* models incorporate the TME, observing cells in real-time to understand their exact role is difficult. Horizontal compartmentalised microfluidic models are a promising new platform for metastasis studies. These devices, composed of adjacent microchannels, can incorporate multiple cell types within a 3D space. Furthermore, the transparency and thickness of these models also enables high quality real-time imaging to be performed. This paper demonstrates how these devices can be successfully used for oral squamous cell carcinoma (OSCC) metastasis studies, focusing on the role of the vascular system in this process. Conditions for co-culture of OSCC cells and endothelial cells have been determined and staining protocols optimised. Furthermore, several imaging analysis techniques for these models are described, enabling precise segmentation of the different cell types on the images as well as accurate assessment of their phenotype. These methods can be applied to any study aiming to understand the role of microenvironmental cell types in cancer

Open Peer Review

Approval Status ✓ ✓

|	1	2
version 2 (revision) 15 Jan 2024	✓ view	✓ view
version 1 25 Apr 2023	? view	? view

1. **Vivek Thacker** [ID], Universitat Heidelberg (Ringgold ID: 9144), Heidelberg, Germany

2. **Christopher Jon Hanley**, University of Southampton, Southampton, UK

Any reports and responses or comments on the article can be found at the end of the article.

metastatic dissemination, and overcome several challenges encountered with current *in vitro* and *in vivo* models. Hence, this new *in vitro* model capable of recapitulating important aspects of the cellular complexity of human metastatic dissemination can ultimately contribute to replacing animal studies in this field.

Keywords
microfluidic, cancer, metastasis, vasculature, HUVEC, microenvironment, chip
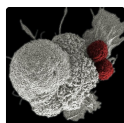
This article is included in the Oncology gateway.

This article is included in the NC3Rs gateway.

Corresponding author: Adrian Biddle (a.biddle@qmul.ac.uk)

> **REVISED** **Amendments from Version 1**
>
> This is a methods paper to accompany a research article that is now available as a pre-print (Scemama *et al.*, 2024). Whilst conducting patient validation of the data from the microfluidic device for the main research article, we wanted to publish the method without delay as a resource for the research community. We have now updated this methods paper to link it to the pre-printed research article. We have also addressed comments from the reviewers, and added Sophia Lunetto as an author. Sophia Lunetto is one of the principal developers of the data analysis applications presented here. In revision, Sophia updated the description of these applications to incorporate her own innovations.
>
> **Any further responses from the reviewers can be found at the end of the article**

Research highlights

Scientific benefits

- Development of a new *in vitro* model to study OSCC metastasis via the vascular system

- Co-culture of different cell types in a 3D matrix, making it more biologically relevant than existing models

- Ability to produce an 'all human' cellular environment – more disease relevant

- High quality imaging, including the ability to study metastatic events in real time at the cellular level

3Rs benefits

- Replacement of animal models for metastasis studies, which are moderate to severe procedures (including chemically induced and xenograft mouse tumour models)

Practical benefits

- Use of cell lines, allowing better reproducibility

- Number of channels and overall design of the device can be amended by the user

Current applications

- Disease modelling of OSCC metastasis

  - Investigating interaction of endothelial and OSCC cells in metastasis

  - Modelling progression of metastasis

Potential applications

- Scale-up the complexity by adding more cells of the tumour microenvironment (e.g. immune cells, lymphatic cells, etc.) as well as additional ECM types, to understand the role of the tumour microenvironment in controlling tumour metastatic behaviour

- Use patient samples to allow a more personalised approach to cancer treatment development

- Use for testing the efficacy of novel drug compounds and/or combinations

---

Introduction

Head and neck squamous cell carcinoma (HNSCC) is the sixth most common malignancy worldwide (Johnson *et al.*, 2020), of which the major sub-type oral squamous cell carcinoma (OSCC) accounts for more than 300,000 cases every year (Choi and Myers, 2008). HPV infections remain a significant driver of OSCC (Jiang and Dong, 2017), as well as tobacco smoking and alcohol misuse. These induce genetic changes in the cells of the oral cavity, eventually leading to the formation of a carcinoma (Rivera, 2015; Scully and Robinson, 2016). OSCC is a type of cancer recognised to have a high impact on the patient's quality of life, as aesthetic defects, as well as chewing and swallowing disabilities, can be induced by the disease and subsequent treatments administered (Rivera, 2015; Sasahira and Kirita, 2018). No radical change has been observed in the treatment landscape for OSCC over the past few decades, with surgery, radiotherapy and chemotherapy remaining the main options offered to patients (Kerawala *et al.*, 2016). Hence, the overall five-year survival for OSCC has remained at around 50% (Scully and Robinson, 2016; Sasahira and Kirita, 2018).

More than 50% of patients with OSCC experience metastasis (Choi and Myers, 2008), with the primary site being the lymph nodes of the neck (Pisani *et al.*, 2020). Metastasis is a complex process where cancer cells must detach from the primary tumour and reach the lymphatic system and/or the blood system to travel to the lymph node and/or distant sites,

such as the lungs, bones and liver (Pisani *et al.*, 2020). Hence, understanding how these cancer cells reach and utilise the vascular system to create these deadly secondary tumours would allow the development of better targeted treatments which prevent this state of the disease from being reached.

In vivo models have been extensively used for OSCC studies. For instance, exposing rodents to molecules including 4-Nitroquinolone oxide (4NQO) or Dimethyl-1,2,benzanthracene (DMBA) can mimic the effect of tobacco and lead to the development of tumours similar to human OSCC (Ishida *et al.*, 2017; Sequeira *et al.*, 2020). Genetically engineered mice have also been utilised with, for instance, Vitale-Cross *et al.* (2004)'s mouse model overexpressing K-ras via keratin 5 and keratin 14 promoters, leading to the development of oral lesions (Vitale-Cross *et al.*, 2004). Xenografts have also been extensively used for metastasis studies, as these have enabled direct study of human cancer cells in immunocompromised rodents. However, the absence of the tumour's native environment and the lack of immune cells in these models remain significant limitations of xenografts for metastasis studies. Furthermore, all these *in vivo* models have additional limitations, including their poor capture of physiological and pathological processes occurring in a human context, ethical drawbacks, high costs, length of studies and the challenges with imaging (Scemama, Lunetto and Biddle, 2022).

Unlike *in vivo* models, *in vitro* models allow high throughput studies to be performed, at a lower cost and without ethical drawbacks. For instance, by forming an endothelial layer on a membrane, transwells have enabled assessment and quantification of cancer cell ability to cross this vascular barrier (Katt *et al.*, 2016). However, real-time imaging of these events remains challenging with these assays, primarily due to issues with barrier opacity and the requirement to image through the construct. More complex *in vitro* models have been developed over the past few years, notably with the emergence of commercialised 3D matrices. For instance, spheroids, recognised as aggregation of cancer cells, present features of tumours and integrate cancer cell-cell interactions in a 3D environment (Katt *et al.*, 2016; Suryaprakash *et al.*, 2020). However, despite the advances of the *in vitro* field, the study of spatial organisation and interactions between different cell types in a 3D space remains limited.

Microfluidic devices are a promising tool for metastasis studies. Since the development of the lung-on-a-chip model (Huh *et al.*, 2010), multiple types of microfluidic devices have emerged in the biomedical research field, including microfluidic membranes, microfluidic scaffolds, microfluidic hydrogels, organ-on-a-plate and horizontal compartmentalised microfluidic devices (Zhang *et al.*, 2018). This article focuses on horizontal compartmentalised microfluidic devices, as these appear highly suited for the study of the interactions between OSCC cells and the vasculature during metastasis. Indeed, these devices are composed of adjacent channels in which different cell types and extracellular matrices (ECMs) can be added. The level of complexity of these models can be modulated by the users, therefore enabling assessment of the effect of specific cells, matrix components and secreted proteins on the cancer cells' phenotype simultaneously or independently (Scemama, Lunetto and Biddle, 2022). Furthermore, the small size of these chips allows high quality imaging to be performed and interactions between cancer cells and microenvironmental cells can be followed in real-time.

Microfluidic devices remain a relatively new model in the biomedical research field, and require the introduction of materials, such as polydimethylsiloxane (PDMS), with inherently abnormal bioactivity compared to more traditional hydrogels such as collagen or fibrin matrices. Therefore, careful optimisation of the assay is required (Rothbauer, Zirath and Ertl, 2018; Sosa-Hernández *et al.*, 2018). This paper describes how this model has been optimised for the co-culture of human endothelial cells with human OSCC cell lines in a three-channel microfluidic device, to better understand the role of the interactions between these two cell types during OSCC metastasis. This methods paper is linked with an associated research article, now available as a pre-print (Scemama *et al.*, 2024), where we use horizontal microfluidic devices to elucidate the effect of the vasculature on the invasive behaviour of OSCC cancer stem cells.

Methods
HUVEC cell culture
Human umbilical vein endothelial cells (HUVECs, **Lonza**, cat. no. **C2519A; RRID**: CVCL_2959) were obtained from Lonza and cultured in EGM-2 medium (Promocell) at 37°C with 5% CO_2. Cells were passaged when a 70–80% confluence was reached. To passage the cells, a wash with phosphate buffered saline (PBS) was first performed and cells were detached using 0.05% Trypsin-EDTA 1X (2.5 ml per T75 flask, Sigma) for 1.5 minutes. EGM-2 was then added to neutralise the trypsin. Cells were used until passage six.

OSCC cell culture
OSCC cells (see Table 1 below for details) were cultured at 37°C with 5% CO_2 in Dulbecco's Modified Eagle Medium (DMEM)-F12 (1:1) + GlutaMAX (31331093, Thermofisher Scientific), supplemented with 10% Fetal Bovine serum (FBS, FB-1001, Biosera), 1% Penicillin-Streptomycin (Pen-strep, Sigma-Aldrich) and 1% RM+ (composed of 10 ng/ml Epidermal Growth Factor [EGF-1, Serotec], 10^{-10} M Cholera Toxin [Sigma-Aldrich], 0.4 µg/ml Hydrocortisone

Table 1. Cell line details.

Cell line	Description
CA1	Human cell line derived from OSCC by Ian Mackenzie lab *Location:* floor of the mouth *HPV:* negative Also available with GFP tag

[Sigma-Aldrich], 5 μg/ml Insulin [Sigma-Aldrich], 5 μg/ml Transferrin [Sigma-Aldrich], 2×10^{-11}M 3,3′,5-Triiodo-L-Thyronine Sodium Salt [Sigma-Aldrich] in DMEM-F12 medium). Cells were passaged when a 70% confluence was reached, by washing them with PBS and detaching them using 0.05% Trypsin-EDTA 1X (Sigma). Once detached, growth medium was added to neutralise the trypsin. Cells were used only at low passage from frozen stocks (up to approx. passage eight), and discarded if gross changes in cell and colony morphology in tissue culture were observed. Retroviral transduction for production of a GFP tagged CA1 OSCC cell line was performed previously (Gemenetzidis *et al.*, 2015).

Microfluidic chip fabrication

The microfluidic chip pattern was designed on AutoCAD® and printed as a film photomask. The device was composed of three channels (700 μm width, ~75 μm height), separated from each other by an array of trapezoidal posts which prevent gel leakage into the side channels whilst allowing cells and signalling molecules to move freely across (100 μm base, 100 μm apart, Figure 1A).

To fabricate the device, a silicon wafer bearing the positive pattern of the chip was generated by photolithography. First, the wafer (PI-KEM) was washed, using acetone and isopropan-2-ol, and dried with nitrogen gas. The wafer was
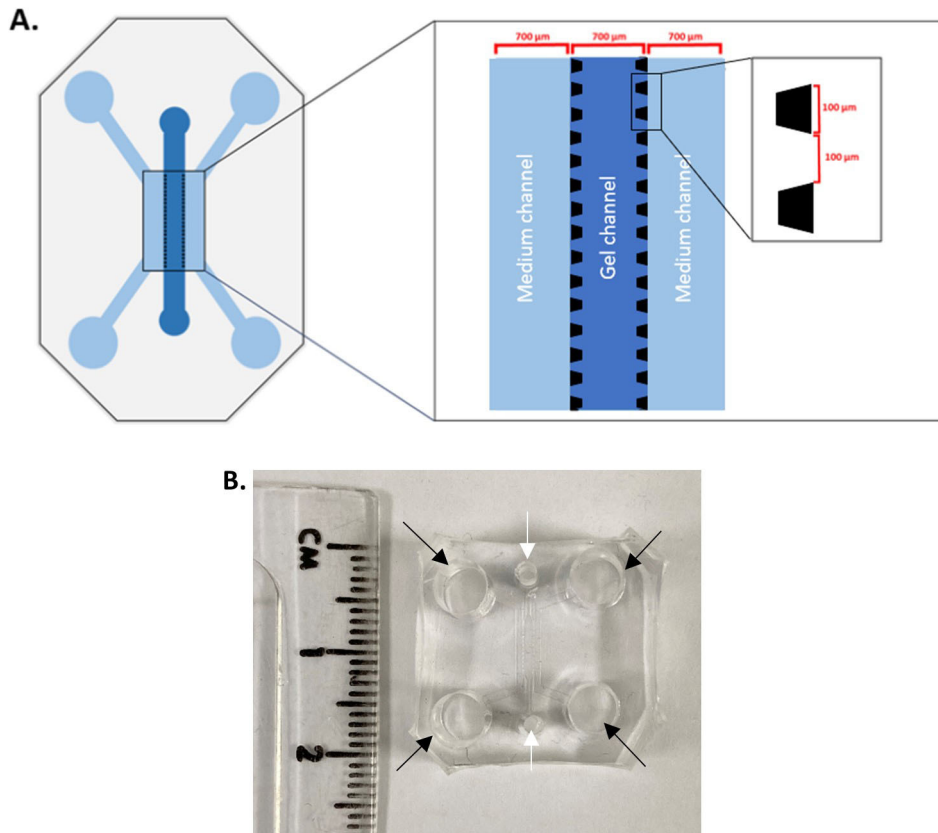
Figure 1. Microfluidic device structure. A. 3-channel microfluidic chip device. Medium is added in the side channels whereas the gel is added in the middle channel. Each channel width is 700 μm, and the height is 75 μm; this enables a minimal working distance from the coverslip. The side channels are delineated from the middle channels by an array of posts, which are 100 μm large and 100 μm apart. B. A cut out PDMS block with side channel inlets (black arrows) and central inlets (white arrows), showing the size of the microfluidic device. It will be bonded to a glass cover slip on the bottom.

then spin-coated with SU-8 2050 photoresist (Kayaku Advanced Materials), by using the following spinning protocol: 500 RPM for 15 seconds with an acceleration of 100 RPM/s and 1700 RPM for 36 seconds with an acceleration of 300 RPM/s. Soft bake was performed by heating the wafer at 65°C for five minutes and 95°C for 15 minutes. The photomask, bearing the pattern of the chip, was placed on the wafer and exposed to UV light (45 mW/cm^2) for one second. The wafer was then heated at 65°C for five minutes and 95°C for 10 minutes, before being immersed in the developing solution, propylene glycol methyl ether acetate (PGMEA, Sigma-Aldrich), for a maximum of five minutes. Finally, a hard bake was conducted by exposing the wafer at 150°C for three minutes.

The resulting silicon wafer bearing the pattern of the desired chip was placed in a petri dish, covered with PDMS and left to set at 80°C. Once crosslinked, the PDMS block was cut out so that new PDMS could be poured onto the silicon wafer, to make new blocks. Blocks were cleaned using ispropan-2-ol and sealed to a glass coverslip via plasma bonding, to close the microchannels. Devices were placed at 80°C for three days, to allow the hydrophobicity of the PDMS to recover, and autoclaved before use for cell culture assays.

Cell culture in the microfluidic device

A fibrin gel was prepared using fibrinogen from bovine plasma (10–15 mg/ml in PBS, Sigma) and thrombin from bovine plasma (5 U/ml in PBS, Sigma-Aldrich). The gel was added in the middle channel via one of the two inlets and pipetted down at a slow pace to prevent leakage (Figure 2i, ii). The gel was left to set at 37°C for 30 minutes, before adding medium to the side channels.

As bubbles may assemble around the posts soon after the addition of medium to the side channels, the devices were left at 37°C overnight to allow these bubbles to dissolve. Medium was then aspirated from all the side channels inlets and 8 μl of a 5 million cells/ml HUVECs suspension was added to one of the inlets of the left side channel (Figure 2iii). To allow cells to adhere to the gel interface, the devices were flipped at 90° for 30 minutes. EGM-2 medium was supplemented with VEGF (50 ng/ml, Peprotech) and added to all the side channels. To enhance sprouting of the HUVECs, to form a developing vascular network within the gel, a flow against the cells was set up by increasing the volume of medium added
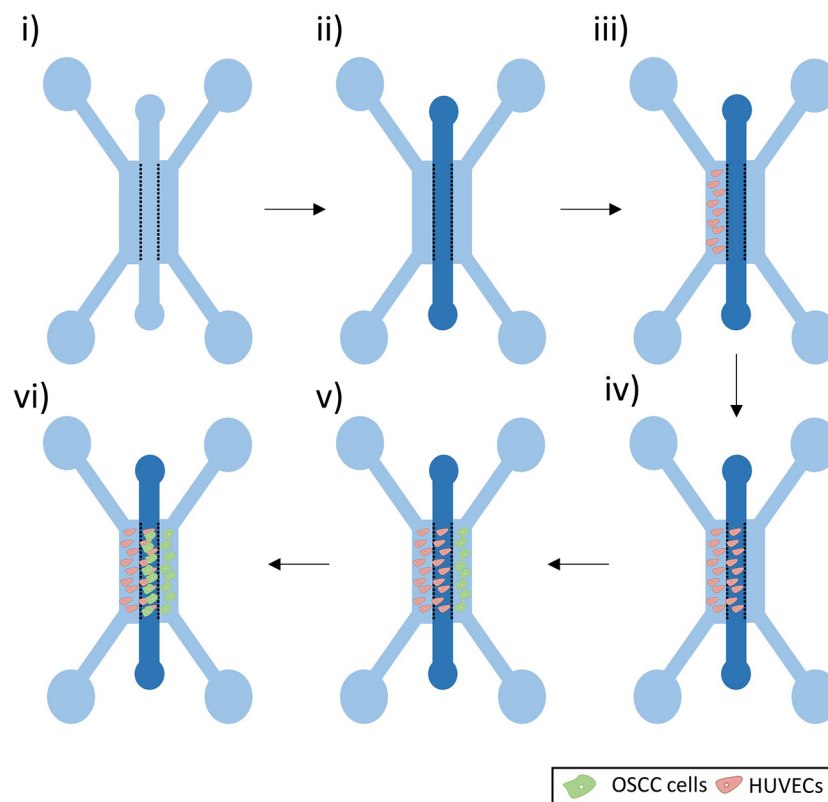
Figure 2. Co-culture experiment set-up. i) Microfluidic Device. ii) A fibrin gel was added in the middle channel. iii-iv) HUVECs were seeded in the left side channel and left to grow in the fibrin gel of the middle channel. v-vi) OSCC cells were then seeded in the right side channel and left to grow in the middle channel.

in the opposite side channel (110 µl of medium in the inlets of the right side channels and 90 µl of the medium in the inlets of the HUVECs side channel). Medium was replaced every 24 hours.

When a vasculature was formed (after approx. four days) (Figure 2iv), OSCC cells were added in the opposite side channel (Figure 2v). Medium was aspirated from all the side channel inlets and 8 µl of a 5 million cells/ml OSCC solution was added to one of the inlets of the right side channel. To allow cells to adhere to the gel interface, the devices were flipped at 90° for 30 minutes. EGM-2 medium supplemented with VEGF (50 ng/ml, Peprotech) was added to both medium channels. Note that DMEM-F12 was not used in the co-culture, to allow the maintenance of endothelial cells in the device.

When the desired time-point of co-culture was reached (Figure 2vi), cells were washed twice with PBS and fixed by adding 100 µl of 4% paraformaldehyde (PFA) in all the inlets for 15 minutes. Cells were washed twice with PBS and left in PBS at 4°C until stained and imaged.

Staining and imaging

Staining reagents were added into both medium channels. Cells were permeabilised with 0.1% Triton X-100 (Sigma-Aldrich) for 10 minutes and blocked for three hours (3% BSA in PBS), at room temperature. If stained with phalloidin (1/500, Scientific Laboratory Supplies) and DAPI (1/1000 in PBS from 1 mg/ml stocks, 10236276001, Roche) or just DAPI, these stains were mixed with the blocking buffer directly and added in each microfluidic chip inlet (100 µl per inlet) for one hour, at room temperature. Cells were washed twice with PBS and left in PBS at 4°C until imaged. When conjugated antibodies were used (see Table 2, below), the antibody mix was prepared using blocking buffer. After the blocking step, 60 µl of the antibody mix was added in each inlet of the microfluidic chips and left overnight at 4°C. Cells were then stained with DAPI for one hour, washed twice with PBS and left in PBS at 4°C until imaged.

Imaging was performed using the IN Cell Analyzer 6000 (GE healthcare). Five to six fields of views, using the 20× magnification, were taken to cover the entire middle channel.

Detailed protocols
Photolithography

Please note: SU8-2050 is light sensitive, steps 1 to 6 need to be conducted in the dark and under a fume hood

1. Clean the silicon wafer (WAFER-SILI-0006W25, PI-KEM) with acetone (100%, 8003, Avantor) and isopropan-2-ol (>99.98%, 59300M, Sigma-Aldrich) and dry it with N_2 gas.

2. Add SU8-2050 (Y111072 0500L1GL, Kayaku Advanced Materials) in the centre of the silicon wafer and slightly tilt at different angles to spread the SU8-2050 on ~70% of the silicon wafer.

3. Place the silicon wafer in the spin coater machine (SPIN150i/200i infinite spin coater, Polos) and start the following programme:

   - Step 1: 500 revolutions per minute (RPM), 15s, acceleration: 100 RPM/s

   - Step 2: 1750 RPM, 36s, acceleration: 300 RPM/s

4. Place the silicon wafer on a heating plate (Isotemp®, *fisher*brand) at 65°C for five minutes and 95°C for 15 minutes. Ensure the silicon wafer is kept in the dark as SU8-2050 is light-sensitive.

5. Place the photomask (bearing the desired chip design) on the silicon wafer and put it in the UV machine (UV-KUB 6) for one second (exposure: 100%; ~45 45 mW/cm^2).

Table 2. Antibody details.

Antibody	Clone	Fluorophore	Company	Reference	RRID	Dilution
Vimentin	V9 (mouse monoclonal)	Alexa Fluor 488	Abcam	ab195877	AB_2916318	1:500
Pan-Cytokeratin	C-11 (mouse monoclonal)	Alexa Fluor 647	Biolegend	628604	AB_2563652	1:100

6. For the post-exposure bake, place the silicon wafer on a heating plate at 65°C for five minutes and 95° for 10 minutes.

7. Under a fume hood, immerse the silicon wafer in the developing solution, PGMEA (484431, Sigma-Aldrich). If the silicon wafer is immersed in it for too long, it will become over-developed and the chip design will disappear. It is preferred to immerse the silicon wafer for 1.5 minutes and then use a squeeze bottle to better target the areas that need to be developed. During this process, regularly wash the silicon wafer with isopropanol.

8. For the hard bake, place the silicon wafer bearing the chip design on a heating plate at 150°C for three minutes.

PDMS pouring and plasma bonding

1. Place the wafer with the desired chip design in a petri dish.

2. Mix polydimethylsiloxane (PDMS; SYLGARDTM 184 Silicone Elastomer Base, Dow Chemical) with its curing agent (SYLGARDTM 184 Silicone Elastomer Curing Agent, 1:10 curing agent to PDMS) and pour it in the petri dish (~1 cm thick). Ensure this is combined well. Once satisfactorily combined, place in a desiccator for 30 minutes for degassing, at room temperature.

3. Pour this in the petri dish (~1 cm thick).

4. Place the petri dish in an oven at 80°C for at least 1.5 hours to allow the PDMS to crosslink.

5. Cut out the solidified blocks of PDMS bearing the chip pattern, using a scalpel, use punch biopsy equipment to create inlets, e.g. 5 mm punch biopsy for side channel inlets and 2 mm punch biopsy for central channel inlets (see Figure 1B).

6. Clean the PDMS blocks by first removing the dust using tape and then immersing them in dH$_2$O and isopropan-2-ol sequentially and drying them with N$_2$ gas in a fume hood.

7. Place the PDMS blocks and 24 × 24 mm (thickness 0.13–0.16 mm) borosilicate glass cover slips in the plasma machine (HPT-200, Henniker Plasma machine) for one minute and seal the channels by placing the PDMS and glass in full contact whilst maintaining a light pressure for 1s.

8. Incubate the devices at 80°C for 72 hours to allow the hydrophobicity to be recovered.

9. Autoclave the devices before using them for cell-based experiments.

Addition of the gel in the microfluidic chips

1. Dilute the fibrinogen type I-S from bovine plasma (F86-30, Sigma) in sterile phosphate buffered saline (PBS) to reach the desired concentration (10–20 mg/ml depending on the fibrinogen batch, each tested to determine the concentration that maintains a consistent degree of angiogenic sprouting) and leave the Eppendorf in the water bath at 37°C for one hour.

2. Filter the fibrinogen solution with a 0.22 μm filter to sterilise it.

3. Prepare the thrombin (T6634, Sigma) by diluting it in sterile PBS to reach the desired concentration (5 U/ml)

4. In a 0.5 ml Eppendorf, add 10 μl of the fibrinogen solution and then add 10 μl of the thrombin solution. Mix it by doing two up-and-downs with the pipette and slowly pipette 10 μl into one of the inlets of the middle channel. Note that less than 10 μl is needed to fill the middle channel, but using higher volumes enables the user to pipette more slowly into the inlet and therefore prevents leakage of the gel to the side channels.

5. Leave the gel to set for 30 minutes at 37°C.

6. Add 100 μl of medium to the top inlets of the side channels.

7. To ensure medium goes through the side channel, cut a 200 μl pipette tip and use it to aspirate the medium via the bottom inlet.

8. Add 100 μl of medium to the bottom inlets of the side channels. At this stage, bubbles may form alongside the gel interface. Leave the microfluidic chips overnight at 37°C to allow the bubbles to disappear before adding the cells into the devices.

<u>Addition of the cells in the microfluidic chips</u>

1. Transfer your cell suspension into a 50 ml falcon and centrifuge it at 1200 RPM for five minutes.

2. Re-suspend in 5 ml of growth medium and count the cells (e.g. using a haemocytometer).

3. Centrifuge the cell solution at 1200 RPM for five minutes and re-suspend in growth medium to reach a final concentration of 5 million cells/ml (note that this may vary depending on the cell type used and desired length of the assay).

4. Remove and discard the growth medium from the inlets of the side channels of the microfluidic chips using an aspirator. All the medium must be aspirated but the channels must not become dry (if dry, the cells will not move towards the gel interface and instead stay in the inlet).

5. Add 8 μl of the cell solution in one of the inlets of a side channel and rotate the device such that the long axis of the channels is parallel with the workbench and the cell solution inlet is superior, in the vertical plane, to the inlets of the opposite side channel. Ensure the device remains in this vertical position for 30 minutes at room temperature to allow the cells to adhere to the gel interface.

6. If the cells have adhered homogeneously to the gel interface, add growth medium in all the inlets of the side channels. In some instances, an interstitial flow can be added, for instance to enhance sprouting of endothelial cells. In that case, a higher volume of growth medium must be added in one of the side channels (for HUVECs: 110 μl in the inlets of the opposing side channel and 90 μl in the inlets of the cells' side channel).

7. Place the devices at 37°C and 5% CO_2.

8. Replace the growth medium every 24 hours.

9. Repeat steps 1–8 to place an additional cell population in the opposite side channel (e.g. cancer cells).

Developer toolbox (GE Healthcare, version 1.10) protocols

In the following, the parameters for the two image analysis protocols in Developer Toolbox (GE Healthcare) are described, allowing the reader to recreate the protocol in the software. Applying a step-by-step process, the software allows the user to interactively adapt parameters to achieve optimal segmentation. In each step, a specific target is segmented using the user's chosen algorithm, then postprocessing steps are applied to refine the segmentation, and lastly measures for the target are identified. Once target objects are segmented, they can be used to identify other targets in the following steps.

Segmentation algorithms include object segmentation, nuclear segmentation, and intensity segmentation. Object segmentation is kernel-based; kernel size and intensity sensitivity (i.e. minimum object brightness-to-background brightness ratio) are chosen by the user. The nuclear segmentation algorithm segments into rounded or octagonal objects using a minimum target area and sensitivity given by the user. Lastly, intensity segmentation identifies objects based on an intensity range defined by the user allowing any object size.

Post-processing steps used here include binary erosion, clump breaking, hole filling and a binary sieve. Binary erosion allows the user to smooth object boundaries using a kernel. Clump breaking utilises a second target to create segmentation between objects. For example, when clump breaking is applied to the 'GFP cells' target, the distance between the nuclei targets is calculated and segmentations are made at equal distances. Hole filling removes exclusions from objects, and the sieve removes objects larger or smaller than a user-defined area threshold.

After object segmentation of various targets, targets are linked to create the final cell objects. In this case, cell targets are linked to the nuclei targets. Any cell object that does not overlap with a nucleus object by at least 80% is removed, to ensure that all cell objects are nucleated.

<u>Protocol 1</u>

The following protocol was used in image analysis to segment two cell types in each field of view. One cell type was GFP-tagged (*GFP cells*). All the cells were stained with phalloidin (red fluorophore). Hence, two groups of cells were segmented: the red-only cells and the red and green cells.

Here, a 'seed' target is used to optimise nuclei segmentation. In this case, a seed target describes a small object located at the brightest part of the nucleus. By using a seed, the algorithm receives a starting point for nuclei segmentation, which improves segmentation performance compared to seedless segmentation. Next, GFP-positive cells were segmented based on their GFP fluorophore intensity. Then, all cells were segmented (*Cells*) based on the phalloidin intensity. GFP-negative cells were segmented by subtracting the *GFP cells* target from the *Cells* targets.

Target sets

- *Seed*

  - Channel: DAPI

  - Object

    - Kernel size: 15

    - Sensitivity: 50

  - Post processing

    - Erosion (Binary):

      - Kernel size: 16

    - Sieve (Binary) - greater than: 20 pixels

- *Nuclei*

  - Channel: DAPI

  - Nuclear segmentation

    - Minimum target area: 600 pixels

    - Sensitivity: 15

  - Post processing

    - Clump breaking – second segmentation: seed

    - Fill holes

    - Sieve (Binary) - less than

    - Sieve (Binary) - greater than

- Measure
  - Sum of Nuclei
- *GFP cells*
  - Channel: FITC
  - Intensity segmentation
  - Post processing
    - Erosion (Binary)
    - Clump breaking – second segmentation: nuclei
    - Fill holes
    - Sieve (Binary) - less than
    - Sieve (Binary) - greater than
- *Debris*
  - Intensity segmentation
  - Post processing
    - Sieve (Binary) - less than
- *Cells*
  - Intensity segmentation
  - Post processing
    - Erosion
    - Clump breaking – second segmentation: nuclei
    - Fill holes
    - Sieve (Binary) - less than
    - Sieve (Binary) - greater than
- *GFP negative cells*
  - Pre-processing macro – P.Sub_11_10_9*
  - Intensity segmentation: Minimum (1); Maximum (65535)
  - Post processing
    - Sieve (Binary) - greater than

- *Whole GFP negative cells*

  - Measure

    - Count Whole GFP negative cells

    - Sum count Whole GFP negative cells

    - Area covered by Whole GFP negative cells

    - Sum area covered by Whole GFP negative cells

- *Whole GFP positive cells*

  - Measure

    - Count Whole GFP positive cells

    - Sum count Whole GFP positive cells

    - Area covered by Whole GFP positive cells

    - Sum area covered by Whole GFP positive cells

Target linking

- *Whole GFP negative cells*

  - Primary target set: Nuclei

  - Secondary target set: GFP negative cells

  - Criteria: overlap

  - Output: Whole GFP negative cells

  - Overlap: 80% of primary target within secondary target

  - Find any matched target

- *Whole GFP positive cells*

  - Primary target set: Nuclei

  - Secondary target set: GFP positive cells

  - Criteria: overlap

  - Output: Whole GFP positive cells

  - Overlap: 80% of primary target within secondary target

  - Find any matched target

* Note: this step allows to subtract all the *GFP cells* target from the *Cells* target to segment the red-only cells. The end image result of *Cells*, *GFP cells* and *GFP negative cells* should be set on the 11th, 10th and 9th windows of the programme respectively. *GFP negative cells* is a subtraction of *GFP cells* (window 10) from *Cells* (window 11).

Protocol 2

The following protocol was used to segment two cell types in each field of view, with two distinct fluorophores. One cell type was GFP-tagged (*GFP cells*), the other was RFP-tagged (*RFP cells*).

Target sets

- *Seed*
  - Object
  - Post processing
    - Erosion (Binary)
    - Sieve (Binary) - greater than

- *Nuclei*
  - Nuclear segmentation
  - Post processing
    - Clump breaking – second segmentation: seed
    - Fill holes
    - Sieve (Binary) - less than
    - Sieve (Binary) - greater than
  - Measure
    - Sum of Nuclei

- *RFP cells*
  - Intensity segmentation
  - Post processing
    - Erosion (Binary)
    - Clump breaking – second segmentation: nuclei
    - Fill holes
    - Sieve (Binary) - less than
    - Sieve (Binary) - greater than

- *GFP cells*

    - Intensity segmentation

    - Post processing

        - Erosion (Binary)

        - Clump breaking – second segmentation: nuclei

        - Fill holes

        - Sieve (Binary) - less than

        - Sieve (Binary) - greater than

- *Whole RFP cells*

    - Measure

        - Count Whole RFP cells

        - Sum count Whole RFP cells

        - Area covered by Whole RFP cells

        - Sum area covered by Whole RFP cells

- *Whole GFP cells*

    - Measure

        - Count Whole GFP cells

        - Sum count Whole GFP cells

        - Area covered by Whole GFP cells

        - Sum area covered by Whole GFP cells

Target linking

- *Whole RFP cells*

    - Primary target set: Nuclei

    - Secondary target set: RFP cells

    - Criteria: overlap

    - Output: Whole RFP cells

    - Overlap: 80% of primary target within secondary target

    - Find any matched target

- *Whole GFP cells*

  - Primary target set: Nuclei

  - Secondary target set: GFP cells

  - Criteria: overlap

  - Output: Whole GFP positive cells

  - Overlap: 80% of primary target within secondary target

  - Find any matched target

Results

Angiogenesis assay

A simple representation of the angiogenesis process was reproduced in the microfluidic chips, by adding HUVECs in the left side channel and leaving them to grow into the fibrin gel in the middle channel. Results showed that endothelial cells formed sprouts in the matrix (Figure 3A). Furthermore, these tubular structures appeared to have a lumen, as when sprouts had grown across the whole middle channel, cells added in the opposite side channels directly migrated into these structures (Figure 3B). Hence, by simply adding HUVECs in our device containing fibrin, we have been able to reproduce a growing vascular network, with features resembling those observed *in vivo*. This is in good agreement with comparable reports of microvascularised chips, presenting lumenated perfusable structures at this time point (Kim *et al.*, 2013; Dibble *et al.*, 2022).

### Co-culture of endothelial cells and OSCC cells to study metastasis

To study the interactions between the OSCC cells and the vasculature, co-culture of HUVECs and OSCC cells was optimised in the microfluidic chip. To allow the discrimination of these two cell types and accurate analysis of the images, GFP-tagged CA1 OSCC cells were used for this experiment (Figure 4). These OSCC cells were added in the opposite side channel when the HUVECs had grown half way across the middle channel, as assessed daily by light microscopy (typically by day 4). Results showed that this co-culture was successful as OSCC cells invaded towards the endothelial cells in the fibrin gel (Figure 4). This successful co-culture will enable the development of experiments to follow and assess the interactions between OSCC cells and the vascular network to better understand the metastasis of OSCC.

Optimisation of the staining

To better understand the interactions between the cancer cells and the vasculature, the expression of specific markers must be assessed. To assess the expression of markers via imaging, such as the lineage markers vimentin and keratin (marking mesenchymal and epithelial lineages respectively), antibodies are required. Non-conjugated antibodies, with primary and
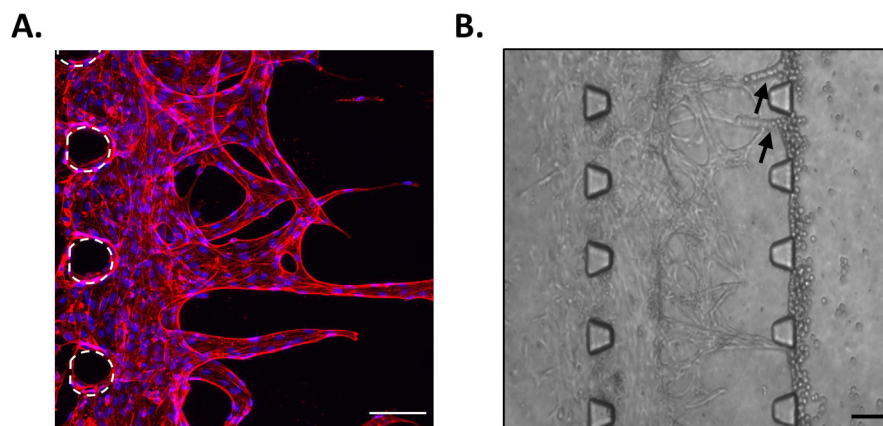
Figure 3. Angiogenesis assay. A. HUVECs in the middle channel of the microfluidic chip at day 10. Red, phalloidin; Blue, DAPI. Posts are highlighted in white (dashed line). Scale bar: 100 µm. B. Migration of CA1 OSCC cells into the sprouts when added in the opposite side channel. Arrows indicate cells that migrated into the sprouts. Scale bar: 100 µm.
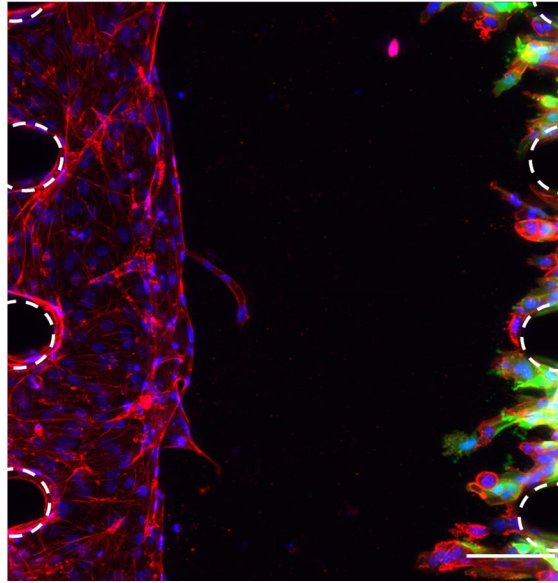
Figure 4. Co-culture of OSCC cells and HUVECs in the microfluidic chip. HUVECs and CA1-GFP OSCC cells in the microfluidic chip 4 days after adding the OSCC cells. Red, phalloidin; Green (GFP tag), OSCC cells; Blue, DAPI. Posts are highlighted in white (dashed line). Scale bar: 100 μm.
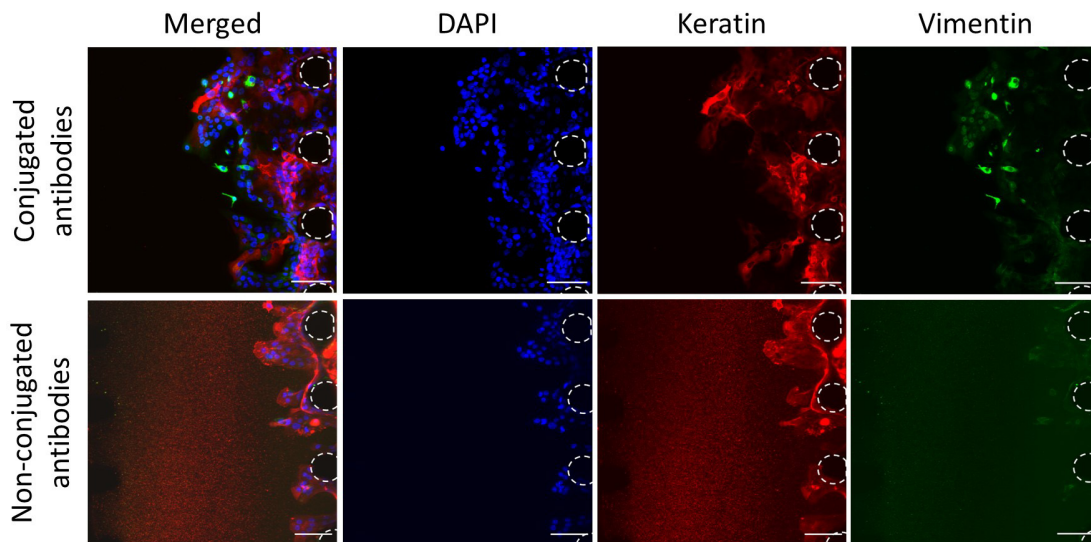
**Figure 5. Optimisation of the staining.** Staining of CA1 OSCC cells with conjugated and non-conjugated antibodies. OSCC cells without vasculature. Red, Keratin; Green, Vimentin; Blue, DAPI. Posts are highlighted in white (dashed line). Scale bars: 100 μm.

secondary antibodies added separately, have been widely used and optimised for imaging in biomedical research. This method allows flexibility over the fluorophore combinations used when multiple marker expressions are being assessed simultaneously. However, when tested in our microfluidic device, high background noise was detected with non-conjugated antibodies, whereas this was not the case with conjugated antibodies (Figure 5). This background noise may reflect some retention of unbound secondary antibodies in the 3D matrix. Hence, this data shows that it may be preferable to use conjugated antibodies in microfluidic devices, to prevent high background noise and thus better analysis of the images obtained.
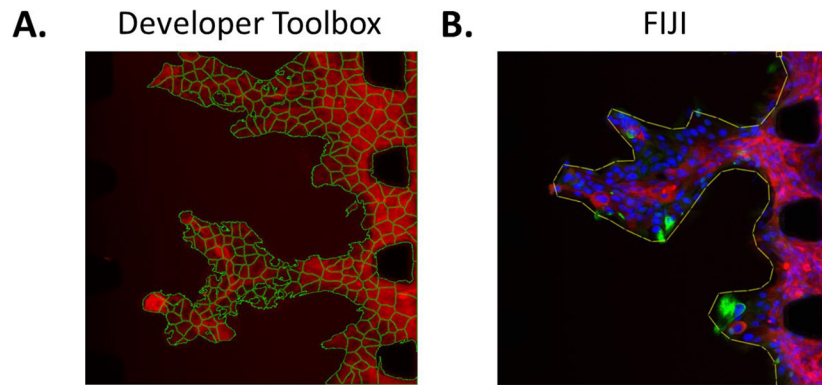
Figure 6. Image analysis method examples. A. Segmentation of each individual CA1-GFP cell using Developer Toolbox. B. Drawing of a region of interest in FIJI (line around the cell mass). CA1 cells stained for Vimentin (green), pan-keratin (red) and DAPI (blue).

Image analysis

Image analysis of the microfluidic chip experiments can be performed using several methods. For instance, for an automated approach, Developer Toolbox (GE Healthcare, version 1.10) can be employed. This programme can segment cells based on their fluorophore intensity and includes a multitude of tools enabling accurate counting of cells, assessment of the area they cover, their X position in the field of view, their shape, etc. (Figure 6A). This automated tool can successfully segment different cell types within a field of view, as long as the cells can be differentiated with a fluorophore. For instance, in Figure 4, cancer cells are GFP-tagged and all the cells are stained with phalloidin (red). Hence, the red-only cells are endothelial cells and the red and green cells are cancer cells. Other tools can also be used for image analysis. For instance, FIJI version 2.9.0 enables drawing of regions of interest manually on each field of view, such as lines surrounding the front of the cell mass, allowing assessment of the complexity of the shape of these masses invading into the matrix (Figure 6B).

Discussion

The number of publications in PubMed featuring the word *organ-on-a-chip* has increased by 80-fold since the start of the century, demonstrating the high interest in this new technology for biomedical research. Indeed, microfluidic devices bring the complexity of *in vitro* models to a new level, by integrating multiple human cell types and enabling study of their interactions in a 3D environment. Furthermore, compared to animal models, microfluidic devices are characterised by their high reproducibility and controllability over the experiments (Ma *et al.*, 2021), while allowing cellular events to be followed in real-time.

Here, a simple model of human OSCC metastasis was developed using horizontal compartmentalised microfluidic devices, with only three elements added to the device: HUVECs, OSCC cells and a fibrin gel. HUVECs were directly purchased from a manufacturer, therefore enhancing the reproducibility of this model; whereas OSCC cells were from patient-derived lines, previously characterised (Biddle *et al.*, 2011, 2016). However, reproducibility of this system was reduced when different fibrinogen batches were used, as the animal origin of this product leads to high batch-to batch variability (Ahadian *et al.*, 2018). Hence, for each new fibrinogen batch used, a range of fibrinogen concentrations should be tested to ensure both HUVECs and OSCC cells exhibit appropriate growth in the device. However, fibrinogen batches do not need to be replaced regularly due to the scale of these devices which allows only small volumes to be used for each experiment. The development of synthetic matrices may also counter this variability, and enables the layering of human matrix components onto the synthetic matrix to generate a fully humanised tumour environment (Ashworth *et al*., 2020). This would further contribute to the 3Rs through reduced experimental variability and reduced reliance on animal derived components.

Conclusions

To conclude, a new *in vitro* model to study the role of the vascular system in the metastasis of OSCC was developed and optimised, aiming to diminish the use of animal models in this field and eventually replace them. This type of device has been used for other cancer types, including breast cancer, glioblastoma, colorectal cancer, etc. (Lee *et al.*, 2014; Jeon *et al.*, 2015; Sobrino *et al.*, 2016), demonstrating its suitability for metastasis studies regardless of the cancer cell origin. In a linked research article, currently pre-printed (Scemama *et al.*, 2024), we have used this device to elucidate the effect of the vasculature on the invasive behaviour of OSCC cancer stem cells. The model developed here has the potential

for up-scaling and adding further complexity, such as additional channels in which additional cell types and/or ECM components could be integrated, to further increase its physiological relevance (Lee *et al.*, 2014, 2018).

Data availability
No data are associated with this article.

References

Ahadian S, *et al.*: **Organ-On-A-Chip Platforms: A Convergence of Advanced Materials, Cells, and Microscale Technologies.** *Adv. Healthc. Mater.* 2018; **7**.
PubMed Abstract | **Publisher Full Text**

Ashworth JC, *et al.*: **Peptide gels of fully-defined composition and mechanics for probing cell-cell and cell-matrix interactions in vitro.** *Matrix Biol.* 2020; **85-86**: 15–33.
Publisher Full Text

Biddle A, *et al.*: **Cancer stem cells in squamous cell carcinoma switch between two distinct phenotypes that are preferentially migratory or proliferative.** *Cancer Res.* 2011; **71**: 5317–5326.
Publisher Full Text

Biddle A, *et al.*: **Phenotypic Plasticity Determines Cancer Stem Cell Therapeutic Resistance in Oral Squamous Cell Carcinoma.** *EBioMedicine.* 2016; **4**: 138–145.
Publisher Full Text

Choi S, Myers JN: **Molecular pathogenesis of oral squamous cell carcinoma: Implications for therapy.** *J. Dent. Res.* 2008; **87**: 14–32.
Publisher Full Text

Dibble M, *et al.*: **Impact of pericytes on the stabilisation of microvascular networks in microfluidic systems in response to nanotoxicity.** *Biorxiv.* 2022.
Publisher Full Text

Gemenetzidis E, Gammon L, Biddle A, *et al.*: **Invasive oral cancer stem cells display resistance to ionising radiation.** *Oncotarget.* 2015; **6**: 43964–43977.
PubMed Abstract | **Publisher Full Text** | **Free Full Text**

Huh D, *et al.*: **Reconstituting organ-level lung functions on a chip.** *Science.* 2010; **328**: 1662–1668.
PubMed Abstract | **Publisher Full Text** | **Free Full Text**

Ishida K, *et al.*: **Current mouse models of oral squamous cell carcinoma: Genetic and chemically induced models.** *Oral Oncol.* 2017; **73**: 16–20.
PubMed Abstract | **Publisher Full Text**

Jeon JS, *et al.*: **Human 3D vascularized organotypic microfluidic assays to study breast cancer cell extravasation.** *Proc. Natl. Acad. Sci. U. S. A.* 2015; **112**: 214–219.
PubMed Abstract | **Publisher Full Text** | **Free Full Text**

Jiang S, Dong Y: **Human papillomavirus and oral squamous cell carcinoma: A review of HPV-positive oral squamous cell carcinoma and possible strategies for future.** *Curr. Probl. Cancer.* 2017; **41**: 323–327.
PubMed Abstract | **Publisher Full Text**

Johnson DE, *et al.*: **Head and neck squamous cell carcinoma.** *Nat. Rev. Dis. Primers.* 2020; **6**: 92.
PubMed Abstract | **Publisher Full Text** | **Free Full Text**

Katt ME, *et al.*: **In vitro tumor models: Advantages, disadvantages, variables, and selecting the right platform.** *Front. Bioeng. Biotechnol.* 2016; **4**.
PubMed Abstract | **Publisher Full Text** | **Free Full Text**

Kerawala C, *et al.*: **Oral cavity and lip cancer: United Kingdom National Multidisciplinary Guidelines.** *J. Laryngol. Otol.* 2016; **130**: S83–S89.
PubMed Abstract | **Publisher Full Text** | **Free Full Text**

Kim S, *et al.*: **Engineering of functional, perfusable 3d microvascular networks on a chip.** *Lab Chip.* 2013; **13**: 1489–1500.
Publisher Full Text

Lee H, *et al.*: **A microfluidic platform for quantitative analysis of cancer angiogenesis and intravasation.** *Biomicrofluidics.* 2014; **8**:
054102.
PubMed Abstract | **Publisher Full Text** | **Free Full Text**

Lee H, *et al.*: **Microfluidic co-culture of pancreatic tumor spheroids with stellate cells as a novel 3d model for investigation of stroma-mediated cell motility and drug resistance.** *J. Exp. Clin. Cancer Res.* 2018; **37**: 4–12.
PubMed Abstract | **Publisher Full Text** | **Free Full Text**

Ma C, *et al.*: **Organ-on-a-Chip: A New Paradigm for Drug Development.** *Trends Pharmacol. Sci.* 2021; **42**: 119–133.
PubMed Abstract | **Publisher Full Text** | **Free Full Text**

Pisani P, *et al.*: **Metastatic disease in head & neck oncology.** *Acta Otorhinolaryngol. Ital.* 2020; **40**(2): S1–S86.
PubMed Abstract | **Publisher Full Text** | **Free Full Text**

Rivera C: **Essentials of oral cancer.** *Int. J. Clin. Exp. Pathol.* 2015; **8**: 11884–11894.
PubMed Abstract

Rothbauer M, Zirath H, Ertl P: **Recent advances in microfluidic technologies for cell-to-cell interaction studies.** *Lab Chip.* 2018; **18**: 249–270.
Publisher Full Text

Sasahira T, Kirita T: **Hallmarks of cancer-related newly prognostic factors of oral squamous cell carcinoma.** *Int. J. Mol. Sci.* 2018; **19**.
PubMed Abstract | **Publisher Full Text** | **Free Full Text**

Scemama A, Lunetto S, Biddle A: **Highlight: microfluidic devices for cancer metastasis studies.** *In vitro Models.* 2022; **1**: 399–403.
Publisher Full Text

Scemama A, Lunetto S, Tailor A, *et al.*: **Hybrid cancer stem cells utilise vascular tracks for collective streaming invasion in a metastasis-on-a-chip device.** *bioRxiv.* 2024; 2024.01.02.573897.
Publisher Full Text

Scully C, Robinson NA: **Oral Cancer.** *International Encyclopedia of Public Health.* 2016.
Publisher Full Text

Sequeira I, *et al.*: **Genomic landscape and clonal architecture of mouse oral squamous cell carcinomas dictate tumour ecology.** *Nat. Commun.* 2020; **11**(1): 5671.
PubMed Abstract | **Publisher Full Text** | **Free Full Text**

Sobrino A, *et al.*: **3D microtumors in vitro supported by perfused vascular networks.** *Sci. Rep.* 2016; **6**.
PubMed Abstract | **Publisher Full Text** | **Free Full Text**

Sosa-Hernández JE, *et al.*: **Organs-on-a-chip module: A review from the development and applications perspective.** *Micromachines.* 2018; **9**.
PubMed Abstract | **Publisher Full Text** | **Free Full Text**

Suryaprakash RTC, *et al.*: **Three-dimensional cell culture models to investigate oral carcinogenesis: A scoping review.** *Int. J. Mol. Sci.* 2020; **21**.
PubMed Abstract | **Publisher Full Text** | **Free Full Text**

Vitale-Cross L, *et al.*: **Conditional expression of K-ras in an epithelial compartment that includes the stem cells is sufficient to promote squamous cell carcinogenesis.** *Cancer Res.* 2004; **64**: 8804–8807.
PubMed Abstract | **Publisher Full Text**

Zhang B, *et al.*: **Advances in organ-on-a-chip engineering.** *Nat. Rev. Mater.* 2018; **3**: 257–278.
Publisher Full Text

F1000Research

Open Peer Review

Current Peer Review Status: ✓ ✓

Version 2

Reviewer Report 21 February 2024

https://doi.org/10.5256/f1000research.161255.r237868

✓ **Christopher Jon Hanley**

University of Southampton, Southampton, England, UK

I have now reviewed the revised version of the manuscript and author response to my comments. With the additional detail provided and reference to the preprint demonstrating specific applications for this method I am happy to now update my status on this article to approved.

Competing Interests: No competing interests were disclosed.

I confirm that I have read this submission and believe that I have an appropriate level of expertise to confirm that it is of an acceptable scientific standard.

Reviewer Report 21 February 2024

https://doi.org/10.5256/f1000research.161255.r237869

✓ **Vivek Thacker** (iD)

Department of Infectious Diseases, Universitat Heidelberg (Ringgold ID: 9144), Heidelberg, Baden-Württemberg, Germany

The authors have addressed my concerns. I would only note that the description for Figure 3B is a little confusing - it is not clear to me exactly what the 'opposite channel' refers to. Are the cancer cells migrating from the left to the right channel? A minor clarification would be helpful.

Competing Interests: No competing interests were disclosed.

Reviewer Expertise: Organ-on-chip, infectious diseases, live-cell imaging

I confirm that I have read this submission and believe that I have an appropriate level of expertise to confirm that it is of an acceptable scientific standard.

- -

Version 1

Reviewer Report 03 August 2023

?

Christopher Jon Hanley
University of Southampton, Southampton, England, UK

This article by Alice Scemama et al. outlines an in vitro approach to modelling metastatic spread in human OSCC, using microfluidic devices that enable high-quality real time imaging. The method describes the fabrication of PDMS moulds with three separate microfluidic channels that can be used for the addition of different cells, matrices or media to the culture. Protocols are also described for imaging-based analysis of these cultures using endogenous fluorophores and/or antibody staining followed by digital analysis involving cell segmentation and quantification of fluorescence intensity.

The method provides useful insight for device fabrication and use for culturing OSCC cells with endothelial cells. As stated by the authors, this device and culture system replicates others that have been used for studying different cancer types previously, so these insights are not entirely novel. It also remains questionable to what degree the stated research highlights are fully achieved by this article.

Conceptual reservations to approval of this article:
- The authors propose that this microfluidic system could be used for investigating the process of OSCC metastasis via the vasculature, suggesting that this could be used instead of animal models. To adequately demonstrate this, further evidence of benchmarking compared to alternative *in vitro* systems and *in vivo* models is required. For example, additional experiments or data that would be useful include:
  - Demonstrating that cell lines with varying metastatic potential *in vivo* exhibit different phenotypes in this model.

  - Demonstrating quantitative metrics can be derived from this model system and the imaging-based analyses proposed to assess these phenotypic differences.

  - Comparing the results generated using this system to a Transwell system or other existing systems (e.g. Ibidi chemotaxis slides).

- The authors highlight real time imaging as a major advantage of this system over existing methods for studying OSCC metastasis. However, the data presented exposes some limitations to these approaches and their utility for progressing the investigation of molecular mechanisms underlying these processes. For example,
  - The use of endogenous fluorophores and phalloidin for classifying different cell types is confounded by non-ubiquitous reporter expression leading to potential for mis-classification of cells, which appears to be the case in the micrograph shown in Figure 4.

  - The interpretation of intercellular interactions across cellular compartments is reliant on strict lineage specific restriction of marker expression. The example provided in figure 5 demonstrates the use of keratin and vimentin "to better understand the interactions between the cancer cells and the vasculature". However, the use of vimentin here is likely to be suboptimal, given this gene is expressed in cancer cells undergoing EMT. The authors should elaborate further on how experiments should be designed to enable accurate examination of tumour vasculature interactions and ensure that the interpretations are validated with appropriate controls.

  - In addition (and as described above) it is not clear how these imaging-based analyses should be used to quantify steps in the metastatic process. Further evaluation and demonstration of how these approaches can be used to measure phenotypic changes under different experimental conditions should be provided to confirm this system be used in a similar manner to existing assays (e.g. Transwell systems) generating reproducible quantitative data.

Technical recommendations/comments:

In the Angiogenesis assay section:

"cells added in the opposite side channels directly migrated into these structures" – clarity should be provided regarding what cells were added to opposite side in this example (Figure 3).

In the Co-culture of endothelial cells and OSCC cells to study metastasis section:

"Results showed that this co-culture was successful as OSCC cells invaded towards the endothelial cells in the fibrin gel" - can the authors explain why angiogenic sprouting was not observed in the cancer cell co-culture? Also, for this statement to be valid it should be shown that invasion into the fibrin gel does not occur in monoculture; in the subsequent figures where OSCC cells are shown alone there is evidence of invasion suggesting this process may be independent of the presence of endothelial cells.

In the Optimisation of the staining section:

"To better understand the interactions between the cancer cells and the vasculature, the expression of specific markers must be assessed" – as described above the markers chosen (keratin and vimentin) are not appropriate for this purpose, use of CD31 or an alternative endothelial cell specific marker should be used. Further clarity should also be provided in the legend for figure 5. Is this example showing OSCC cells grown in monoculture or co-culture?

"This background noise may reflect some retention of unbound secondary antibodies in the 3D matrix." - can the authors provide rationale for why excess secondary antibody but not primary antibody would be retained within the 3D matrix? Could indirect antibody staining be feasible with further optimisation of the staining protocol? If conjugated antibodies must be used instead of indirect antibody staining the feasibility for analysing different proteins in this system is likely to be significantly reduced, due to limited commercial availability of conjugated antibodies and lack of signal amplification.

In the Image analysis section:

The description of cell segmentation and analysis methodology is not adequately described for readers unfamiliar with the developer toolbox software. Clear descriptions should be provided for the algorithms used for cell segmentation. Additionally, it is unclear whether the term cell segmentation is used correctly throughout the article. This process refers to demarcation of cellular boundaries but seems to be used to describe both cell segmentation and cell-type/group classification, which are two distinct processes.

Is the rationale for developing the new method (or application) clearly explained?
Yes

Is the description of the method technically sound?
Partly

Are sufficient details provided to allow replication of the method development and its use by others?
Partly

If any results are presented, are all the source data underlying the results available to ensure full reproducibility?
No source data required

Are the conclusions about the method and its performance adequately supported by the findings presented in the article?
Partly

Competing Interests: No competing interests were disclosed.

Reviewer Expertise: Tumour microenvironment research using 3D cultures, digital pathology and bioinformatics

I confirm that I have read this submission and believe that I have an appropriate level of expertise to confirm that it is of an acceptable scientific standard, however I have significant reservations, as outlined above.

Author Response 10 Jan 2024

Adrian Biddle

This article by Alice Scemama et al. outlines an in vitro approach to modelling metastatic spread in human OSCC, using microfluidic devices that enable high-quality real time imaging. The method describes the fabrication of PDMS moulds with three separate microfluidic channels that can be used for the addition of different cells, matrices or media to the culture. Protocols are also described for imaging-based analysis of these cultures using endogenous fluorophores and/or antibody staining followed by digital analysis involving cell segmentation and quantification of fluorescence intensity.

The method provides useful insight for device fabrication and use for culturing OSCC cells with endothelial cells. As stated by the authors, this device and culture system replicates others that have been used for studying different cancer types previously, so these insights are not entirely novel. It also remains questionable to what degree the stated research highlights are fully achieved by this article.

We thank the reviewer for their encouraging words and thorough review. As mentioned for reviewer 1, this is a methods paper to accompany a research article that is now pre-printed (Scemama et al., 2024). Whilst conducting patient validation of the data from the microfluidic device for the main research article, we wanted to publish the method without delay as a resource for the research community. We have now updated this methods paper to link it to the pre-printed research article. Where comments are addressed in the main research article, we will note that below.

The particular focus of our own work is on using microfluidic devices to study the evolution of tumour cellular heterogeneity and plasticity within a complex tumour microenvironment, and the analysis methods we have developed and presented here are designed to enable the application of microfluidic devices to this area of study.

Conceptual reservations to approval of this article:
- *The authors propose that this microfluidic system could be used for investigating the process of OSCC metastasis via the vasculature, suggesting that this could be used instead of animal models. To adequately demonstrate this, further evidence of benchmarking compared to alternative in vitro systems and in vivo models is required. For example, additional experiments or data that would be useful include:*
  - *Demonstrating that cell lines with varying metastatic potential in vivo exhibit different phenotypes in this model.*
  - *Demonstrating quantitative metrics can be derived from this model system and the imaging-based analyses proposed to assess these phenotypic differences.*
  - *Comparing the results generated using this system to a Transwell system or other existing systems (e.g. Ibidi chemotaxis slides).*

An important advantage of this system is the ability to generate quantitative single-cell metrics, due to the superior imaging over existing *in vitro* and *in vivo* methods. Methods for the generation of such metrics are presented in this methods paper, and we have

presented both the outputs of these methods and patient validation data in the main research article (Scemama et al., 2024). Our focus is on benchmarking against human clinical and pathological data, as *in vivo* animal data is often an inaccurate representation of the clinical truth.

○ *The authors highlight real time imaging as a major advantage of this system over existing methods for studying OSCC metastasis. However, the data presented exposes some limitations to these approaches and their utility for progressing the investigation of molecular mechanisms underlying these processes. For example,*
  ○ *The use of endogenous fluorophores and phalloidin for classifying different cell types is confounded by non-ubiquitous reporter expression leading to potential for mis-classification of cells, which appears to be the case in the micrograph shown in Figure 4.*

Reviewer 1 had the same concern, and we have responded in detail there. Briefly, this concern is due to the inability to display the entire dynamic expression range in an image. The expression is in fact ubiquitous.

○ ○ *The interpretation of intercellular interactions across cellular compartments is reliant on strict lineage specific restriction of marker expression. The example provided in figure 5 demonstrates the use of keratin and vimentin "to better understand the interactions between the cancer cells and the vasculature". However, the use of vimentin here is likely to be suboptimal, given this gene is expressed in cancer cells undergoing EMT. The authors should elaborate further on how experiments should be designed to enable accurate examination of tumour vasculature interactions and ensure that the interpretations are validated with appropriate controls.*

The reference to keratin and vimentin expression here is in relation to the cancer cells, as we are interested in identifying cancer cells undergoing EMT. The vascular cells do indeed also express vimentin, but this can be separated out by including co-localisation with the GFP lineage reporter in the quantitative analysis. This is elaborated further in the associated research article (Scemama et al., 2024).

○ ○ *In addition (and as described above) it is not clear how these imaging-based analyses should be used to quantify steps in the metastatic process. Further evaluation and demonstration of how these approaches can be used to measure phenotypic changes under different experimental conditions should be provided to confirm this system be used in a similar manner to existing assays (e.g. Transwell systems) generating reproducible quantitative data.*

The assessment of changes under different experimental conditions, using the quantitative methods described in this methods paper, is a key feature of the associated research article (Scemama et al., 2024).

Technical recommendations/comments:

In the <u>Angiogenesis assay</u> section:

"cells added in the opposite side channels directly migrated into these structures" – clarity should be provided regarding what cells were added to opposite side in this example (Figure 3).

The cells in the opposite channel were CA1, and we have now clarified this.

In the <u>Co-culture of endothelial cells and OSCC cells to study metastasis</u> section:

"Results showed that this co-culture was successful as OSCC cells invaded towards the endothelial cells in the fibrin gel" - can the authors explain why angiogenic sprouting was not observed in the cancer cell co-culture? Also, for this statement to be valid it should be shown that invasion into the fibrin gel does not occur in monoculture; in the subsequent figures where OSCC cells are shown alone there is evidence of invasion suggesting this process may be independent of the presence of endothelial cells.

Indeed, the invasion of CA1 cells into the device occurs in both the presence and absence of HUVECs. Our point here is that we have established culture conditions that allow the successful co-culture of both cell types within the device such that their interactions can be investigated. Investigation of the effects of this co-culture on both the cancer and endothelial cells is a major focus of the associated research article (Scemama et al., 2024).

In the <u>Optimisation of the staining</u> section:

"To better understand the interactions between the cancer cells and the vasculature, the expression of specific markers must be assessed" – as described above the markers chosen (keratin and vimentin) are not appropriate for this purpose, use of CD31 or an alternative endothelial cell specific marker should be used. Further clarity should also be provided in the legend for figure 5. Is this example showing OSCC cells grown in monoculture or co-culture?

This example of staining is on cells growing in monoculture – this has been added. As we've outlined in a previous answer, vimentin and keratin are both used as markers in the cancer cells. CD31 can successfully mark the endothelial cells, as can an RFP marker (Scemama et al., 2024).

"This background noise may reflect some retention of unbound secondary antibodies in the 3D matrix." - can the authors provide rationale for why excess secondary antibody but not primary antibody would be retained within the 3D matrix? Could indirect antibody staining be feasible with further optimisation of the staining protocol? If conjugated antibodies must be used instead of indirect antibody staining the feasibility for analysing different proteins in this system is likely to be significantly reduced, due to limited commercial availability of conjugated antibodies and lack of signal amplification.

We tried extensive optimisation of indirect antibody staining before proceeding with direct antibody staining so, whilst we cannot know whether it would be feasible with the correct

optimisation, it certainly seems a difficult approach within this system. In contrast, direct antibody staining worked very well. We suggest that, being a 3D system, there is more opportunity for antibody to diffuse away from the intended target than in 2D staining. Certainly, extended time between staining and imaging increases this problem. It may be that the binding of primary antibodies to their target is stronger than the binding of secondary antibodies, with less diffusion away, and of course there is less fluorescence signal overall in the system.

In the past, we have relied on indirect staining due to the signal amplification effect and limited commercial availability of conjugated antibodies. However, these advantages of indirect staining no longer hold. Improved imaging systems and techniques have rendered the signal amplification effect of secondary antibodies unnecessary for our applications, and commercial providers now have greatly improved catalogues of conjugated antibodies (including recombinantly produced antibodies) such that the majority of targets of interest have antibodies available conjugated to a range of fluorophores.

In the _Image analysis_ section:

The description of cell segmentation and analysis methodology is not adequately described for readers unfamiliar with the developer toolbox software. Clear descriptions should be provided for the algorithms used for cell segmentation. Additionally, it is unclear whether the term cell segmentation is used correctly throughout the article. This process refers to demarcation of cellular boundaries but seems to be used to describe both cell segmentation and cell-type/group classification, which are two distinct processes.

We have updated this section to improve the description and clearly define the term 'segmentation'.

References:

SCEMAMA, A., LUNETTO, S., TAILOR, A., CIO, S. D., AMBLER, L., COETZEE, A., COTTOM, H., KHURRAM, S. A., GAUTROT, J. & BIDDLE, A. 2024. Hybrid cancer stem cells utilise vascular tracks for collective streaming invasion in a metastasis-on-a-chip device. *bioRxiv*, 2024.01.02.573897.

Competing Interests: No competing interests were disclosed.

Reviewer Report 15 June 2023

https://doi.org/10.5256/f1000research.144690.r171696

?   **Vivek Thacker** (iD)

Department of Infectious Diseases, Universitat Heidelberg (Ringgold ID: 9144), Heidelberg, Baden-Württemberg, Germany

In this manuscript, Scemama and colleagues describe the design, fabrication, and testing of an organ-on-chip device to visualize the metastasis of patient-derived oral squamous carcinoma cells into vascular networks. The device consists of vascular cells seeded in one channel that form an extended network into the adjacent (central) fibrin-gel containing channel and OSCC cells seeded in the other side channel that interact with the vascular cells in the central channel. The use of such a side-by-side geometry overcomes many of the limitations of layered microfluidic devices. OSCC cells are identified by GFP transduction. Overall, the rationale for the need for such devices is clearly described, and the fabrication processes of the organ-chip device has been described with sufficient detail to enable to reader to replicate these experiments. However, there are shortcomings in relation to the characterization of the devices from a cellular perspective. The availability of patient-derived OSCC cells is a huge asset, but apart from the CA1 line, none of the others described in Table 1 are used in this study. There are several similar designs reported for the culture of vascular networks in co-culture with several other cell types including tumour cells, and the authors should place their device in the context of this work. In addition, the authors do not show evidence for a close co-culture in the central channel between the endothelial and OSCC cells, which is needed if this device is to be used to study metastasis as claimed.

Major comments:

Characterization of GFP-labelled OSCC cells – the data in Figure 4 suggests that several of the GFP labelled cells have low or no GFP expression whereas others have high GFP expression. Did the authors choose one particular clone for expansion or are the cells a mixed population? Protocols for characterization of these cells are important and should be included so as to enable others to repeat these experiments. Furthermore, the lack of GFP expression in a sub-population of OSCC cells is problematic given that this marker is used to classify the OSCC cells in the chip. Are these cells losing GFP expression over the period of growth in the organ-on-chip? The authors could show data with other epithelial markers like EpCAM or E-cadherin to characterize these cells further.

Co-culture on-chip – the manuscript claims in Figures 2 (v) and (vi) that a co-culture of a vascular network and the OSCC cells is possible, but this is not supported by the images in Figures 4, 5, and 6. The timepoint at which the chips are imaged in Figures 4, 5, and 6 are not clear – it is likely that these are early timepoints and there has been insufficient time to generate the co-culture. Evidence from later stages needs to be provided to back up this claim.

Vascular network on-chip – the authors claim on page 14 and in relation to Figure 3 that their protocol generates a perfusable vascular network, but there is no functional evidence provided. Please nuance this claim or provide evidence to support it. Furthermore, the authors do not adequately cite other publications in this field, notably from the lab of Prof Roger Kamm who has created several models that have extensive perfusable vascularization, including with the addition of tumor cells. The authors should place their model in the context of this literature.

Table 1 and OSCC cells – the need for table 1 is unclear since none of the other patient-derived cell lines are used in this study and the protocols that the authors propose requires the use of the

GFP-labelling to identify OSCC cells. Inclusion of the patient-derived cells is a strength, and the authors could significantly strengthen the manuscript by comparing the behaviours of these four cell lines in the same device for parameters such as invasion or growth or spread via metastasis.

Image analysis pipeline – it is unclear how the images generated in Figure 6 are obtained, and how this is useful for the purpose of analysis of metastasis. It is unclear how the cell boundaries in 6A are determined given the low and homogenous GFP expression. This image doesn't quite correlate with the image in 6B, is this a different field of view? In 6B there are very few GFP+ cells, so is this an area from the vascular side of the device? In any case, it does not appear that a vascular network that interacts with many OSCC cells (as depicted in Figure 2 (vi)) has been generated.

<u>Minor comments:</u>
Page 4, limitations of in vivo models - several limitations are described at the top of page 4, it would be useful to have references to these.

Page 4, limitations of transwells – these models are described as unsuitable for real-time imaging. The authors should clarify exactly why (transparency of membrane, working distance etc.) to help the reader assess these limitations.

Page 5, UV light – typo, should be mW and not Mw.

Figure 1 - the schematics are nicely presented, showing an XZ or YZ cross-section would also help the reader appreciate the low working distance from the coverslip afforded by the authors' design.

Page 7 – the details of the vector used for GFP expression are incompletely described. Please describe these and provide references for the vector. Typo – 'polybrene' and not 'prolbrene'.

Figures 3-6 – please avoid the use of primary colours to enable colour-blind readers to appreciate the images.

Is the rationale for developing the new method (or application) clearly explained?
Yes

Is the description of the method technically sound?
Partly

Are sufficient details provided to allow replication of the method development and its use by others?
Partly

If any results are presented, are all the source data underlying the results available to ensure full reproducibility?
Partly

Are the conclusions about the method and its performance adequately supported by the findings presented in the article?

No

Competing Interests: No competing interests were disclosed.

Reviewer Expertise: Organ-on-chip, infectious diseases, live-cell imaging

I confirm that I have read this submission and believe that I have an appropriate level of expertise to confirm that it is of an acceptable scientific standard, however I have significant reservations, as outlined above.

Author Response 10 Jan 2024
Adrian Biddle

In this manuscript, Scemama and colleagues describe the design, fabrication, and testing of an organ-on-chip device to visualize the metastasis of patient-derived oral squamous carcinoma cells into vascular networks. The device consists of vascular cells seeded in one channel that form an extended network into the adjacent (central) fibrin-gel containing channel and OSCC cells seeded in the other side channel that interact with the vascular cells in the central channel. The use of such a side-by-side geometry overcomes many of the limitations of layered microfluidic devices. OSCC cells are identified by GFP transduction. Overall, the rationale for the need for such devices is clearly described, and the fabrication processes of the organ-chip device has been described with sufficient detail to enable to reader to replicate these experiments. However, there are shortcomings in relation to the characterization of the devices from a cellular perspective. The availability of patient-derived OSCC cells is a huge asset, but apart from the CA1 line, none of the others described in Table 1 are used in this study. There are several similar designs reported for the culture of vascular networks in co-culture with several other cell types including tumour cells, and the authors should place their device in the context of this work. In addition, the authors do not show evidence for a close co-culture in the central channel between the endothelial and OSCC cells, which is needed if this device is to be used to study metastasis as claimed.

We thank the reviewer for their enthusiasm for the method presented in our report, and for their thorough review. We will answer the specific comments where they appear below. One thing to note is that this is a methods paper to accompany a research article that is now available as a pre-print (Scemama et al., 2024). Whilst conducting patient validation of the data from the microfluidic device for the main research article, we wanted to publish the method without delay as a resource for the research community. We have now updated this methods paper to link it to the pre-printed research article. Where comments are addressed in the main research article, we will note that below.

Major comments:

Characterization of GFP-labelled OSCC cells – the data in Figure 4 suggests that several of the GFP labelled cells have low or no GFP expression whereas others have high GFP expression. Did the authors choose one particular clone for expansion or are the cells a mixed population? Protocols for characterization of these cells are important and should be included so as to enable others to repeat these experiments. Furthermore, the lack of GFP expression in a sub-population of OSCC cells is problematic given that this marker is used to classify the OSCC cells in the chip.

Are these cells losing GFP expression over the period of growth in the organ-on-chip? The authors could show data with other epithelial markers like EpCAM or E-cadherin to characterize these cells further.

The apparent lack of GFP expression in some OSCC cells in Fig. 4 is due to the fact that the level of GFP expression is over enough of a range that the levels in the lower expressing cells cannot be visualised without making the higher expressing cells too bright. Quantitative analysis of GFP expression compared to a negative control (e.g. HUVEC) demonstrates that it is positive in all of the OSCC cells. It is also positive in all OSCC cells when tested by flow cytometry.

The protocol for production of GFP+ CA1 cells, and their characterisation by flow cytometry, is detailed in the cited publication (Gemenetzidis et al., 2015). We do not use clonal expansion, as the cancer cell line is a heterogeneous population and therefore single cell expansion results in a non-representative population.

EpCAM and E-cadherin expression are investigated in the associated research article (Scemama et al., 2024), and also exhibit a range of expression levels in the OSCC cells.

Co-culture on-chip – *the manuscript claims in Figures 2 (v) and (vi) that a co-culture of a vascular network and the OSCC cells is possible, but this is not supported by the images in Figures 4, 5, and 6. The timepoint at which the chips are imaged in Figures 4, 5, and 6 are not clear – it is likely that these are early timepoints and there has been insufficient time to generate the co-culture. Evidence from later stages needs to be provided to back up this claim.*

The timepoints are noted in the figure legends. The evolution of the co-culture after addition of OSCC cells is the specific focus of the associated research article, and is described in detail there (Scemama et al., 2024). The purpose of this methods article is to describe methods for production of the co-culture devices and for quantitative analysis of the resulting cultures. Briefly, the separation of OSCC cells and HUVECs is due to their response to one another. Allowing more complete vascularisation before adding OSCC cells results in OSCC cells flowing through the vasculature (Fig. 3), which may or may not be desirable depending on study aims.

Vascular network on-chip *– the authors claim on page 14 and in relation to Figure 3 that their protocol generates a perfusable vascular network, but there is no functional evidence provided. Please nuance this claim or provide evidence to support it. Furthermore, the authors do not adequately cite other publications in this field, notably from the lab of Prof Roger Kamm who has created several models that have extensive perfusable vascularization, including with the addition of tumor cells. The authors should place their model in the context of this literature.*

The functional evidence for the production of a lumenised vasculature is the image in Fig. 3B showing cancer cells flowing directly into the vascular lumen. This happens when we allow the vasculature to progress across the whole width of the middle channel and connect to the far side channel, before adding the cancer cells. Usually, we add the cancer cells before the vasculature reaches this level of development, as shown in the other images presented.

We agree that our work builds on important previous work on the development of these microfluidic devices for investigation of cancer interaction with the vasculature. Prof Roger Kamm pioneered these devices, and we have cited his work (Jeon et al., 2015) alongside other key previous studies. This is in the conclusion section in page 17, and in the first results section relating to previous studies demonstrating production of perfusable vascular structures. The particular focus of our own work is on using these devices to study the evolution of tumour cellular heterogeneity and plasticity within a complex tumour microenvironment, and the analysis methods we have developed and presented here are designed to enable the application of microfluidic devices to this area of study.

Table 1 and OSCC cells *– the need for table 1 is unclear since none of the other patient-derived cell lines are used in this study and the protocols that the authors propose requires the use of the GFP-labelling to identify OSCC cells. Inclusion of the patient-derived cells is a strength, and the authors could significantly strengthen the manuscript by comparing the behaviours of these four cell lines in the same device for parameters such as invasion or growth or spread via metastasis.*

The inclusion of cell lines not used in this methods paper was a mistake, and we have now removed them. These are the cell lines used in the associated research article (Scemama et al., 2024), and we agree that the inclusion of multiple patient-derived cell lines is an important consideration for research studies using these devices.

Image analysis pipeline *– it is unclear how the images generated in Figure 6 are obtained, and how this is useful for the purpose of analysis of metastasis. It is unclear how the cell boundaries in 6A are determined given the low and homogenous GFP expression. This image doesn't quite correlate with the image in 6B, is this a different field of view? In 6B there are very few GFP+ cells, so is this an area from the vascular side of the device? In any case, it does not appear that a vascular network that interacts with many OSCC cells (as depicted in Figure 2 (vi)) has been generated.*

These images are of control devices with no vasculature. The purpose of this figure was to show the analysis methods used, we therefore used images of OSCC monoculture to make it easier to follow.

In 6a, the cells are CA1-GFP. This is to show that with fluorescent cells, Developer can easily be used to segment the cells using the nucleus (DAPI staining).

In 6b, the cells are stained with Vimentin/Keratin with Vimentin in green and Keratin in red. The cells used here were normal CA1 (non-GFP CA1) in order to be able to do the double antibody stain.

The legend has been updated to make the above details clear.

These two images are indeed different but this is because the goal was to show two different methods
1) With fluorescent CA1, it is a lot easier to do an automatic segmentation (as shown in 6a).
2) With non-fluorescent CA1, stained for markers, a manual analysis is preferred (6b). Here

we are showing how to calculate the length of the cell front by drawing a line manually.

Minor comments:
Page 4, limitations of in vivo models *- several limitations are described at the top of page 4, it would be useful to have references to these.*

The reference has been moved to make clear it covers all of these limitations. It is a review that covers these in more detail.

Page 4, limitations of transwells – *these models are described as unsuitable for real-time imaging. The authors should clarify exactly why (transparency of membrane, working distance etc.) to help the reader assess these limitations.*

This has been updated with further explanation.

Page 5, UV light – *typo, should be mW and not Mw.*

Updated.

Figure 1 *- the schematics are nicely presented, showing an XZ or YZ cross-section would also help the reader appreciate the low working distance from the coverslip afforded by the authors' design.*

This is a good point; we have edited the legend to add this point.

Page 7 – *the details of the vector used for GFP expression are incompletely described. Please describe these and provide references for the vector. Typo – 'polybrene' and not 'prolybrene'.*

We have re-considered the inclusion of this methods section, as the GFP line was produced as part of a previous study and not by the authors of the current study. We have instead included a reference to the study where the CA1-GFP were produced (Gemenetzidis et al., 2015).

Figures 3-6 *– please avoid the use of primary colours to enable colour-blind readers to appreciate the images.*

Thank you. We will incorporate this point into our future image analysis pipeline.

References

GEMENETZIDIS, E., GAMMON, L., BIDDLE, A., EMICH, H. & MACKENZIE, I. C. 2015. Invasive oral cancer stem cells display resistance to ionising radiation. *Oncotarget,* 6**,** 43964-77.
SCEMAMA, A., LUNETTO, S., TAILOR, A., CIO, S. D., AMBLER, L., COETZEE, A., COTTOM, H., KHURRAM, S. A., GAUTROT, J. & BIDDLE, A. 2024. Hybrid cancer stem cells utilise vascular tracks for collective streaming invasion in a metastasis-on-a-chip device. *bioRxiv***,** 2024.01.02.573897.

The benefits of publishing with F1000Research:

- Your article is published within days, with no editorial bias

- You can publish traditional articles, null/negative results, case reports, data notes and more

- The peer review process is transparent and collaborative

- Your article is indexed in PubMed after passing peer review

- Dedicated customer support at every stage

For pre-submission enquiries, contact research@f1000.com

F1000Research